

Simulating Polymer Drag Reduction Using a Modified Mixing Length in Zero Pressure Gradient Boundary Layers

J. J. White, A. G. L. Holloway, and T. L. Jeans

Department of Mechanical Engineering, University of New Brunswick, Fredericton, Canada

Abstract—It is known that a small concentration of polymer introduced to the boundary layer can produce significant drag reduction for liquid flows. This effect has been studied extensively for internal flow and polymer injection in external flow, though much is still unknown about the underlying mechanism. More recently, select external flow research has focused on drag reduction for ships. The present work is a building block towards a practical methodology for simulating an ablative polymer paint to induce drag reduction on submarine geometries. Polymer drag reduction experiments can be closely reproduced by modifying empirical constants in the simple mixing length turbulence model. Potential avenues for implementation in standard commercially available CFD solvers are explored.

Keywords—Drag Reduction; Boundary Layer; Polymer; Turbulence Model; Flat Plate; CFD

I. INTRODUCTION

Autonomous Underwater Vehicles (AUVs) are increasingly being utilized for seafloor surveying and security in arctic waters. However, a fundamental limitation of AUVs for such applications is their limited range and endurance. Hydrodynamic drag reduction has been the subject of research for decades, resulting in several methods suitable for the AUV application. These include compliant coatings, surface riblets, transition delay, the application of polymer/surfactant additives, and gas micro-bubbles [1]. Of these, viscoelastic polymers are an attractive candidate as they are effective in low concentrations, and it is anticipated that the low vehicle speeds in this application do not produce mechanical degradation of the polymer found at higher shear rates [2], [3]. An ablative polymer paint has recently received full-scale testing on the 176k DWT PAN BONA bulk carrier, where the drag reduction effect was shown to be not negligible [4].

Total drag on a submerged object is composed of pressure and skin friction drag. To simulate the skin friction reduction that is experienced in polymer solutions, shear stress on the wall $\tau_w = \mu \frac{\partial u}{\partial y} \Big|_w$, must be reduced. Modeling this effect has been approached from two different directions in the literature depending on the relative concentration: For relatively high concentrations, it has been approached through shear viscosity, μ , reduction due to shear-thinning non-Newtonian

behavior. In relatively low concentrations, viscoelastic effects are believed to dominate through elastic stretching of the polymer molecule, causing turbulence damping reducing turbulent energy. Attempts have been made to simulate these rheological effects through the significantly more complex finitely extensible nonlinear elastic (FENE) equations [5]–[9]. Both manifest in a reduction in τ_w .

A homogenous polymer concentration is possible for internal flow, with drag reduction effects scaled with polymer concentration up to the maximum drag reduction (MDR) asymptote. Conversely, an ablative polymer dissolving into the flow provides a range of concentrations across the flow field. Therefore, modeling the external flow problem has two components: (1) Accurately tracking the polymer concentration within the flow; a methodology for this has been proposed in [10]. (2) Modifying the flow field as a function of polymer concentration to simulate drag reduction. This paper is a building block towards (2) to determine if accurate drag reduction can be obtained in zero pressure gradient using a simple modification of the mixing length model. As well as exploration of potential avenues for implementation into available computational fluid dynamics (CFD) models.

II. THEORY & DATASET FOR COMPARISON

It is known that a small concentration of polymer in the boundary layer can produce significant drag reduction, as first discovered in 1948 by Toms [11]. This phenomenon has been studied extensively for internal flow; however, much is still not understood about the fundamental nature of polymer drag reduction (PDR). The earliest two-layer models by authors such as Meyer [12] and Elata et al. [13], represent the influence of polymer as a thickening of the viscous sublayer and an upwards shift of the log layer intercept [14]. Improving on this, Virk [15], [16] contributed a three-layer model that can be considered classical PDR theory. It was found that for a sufficiently large polymer concentration, the boundary layer reaches a MDR asymptote, shown in Figure 1a. Virk found that the MDR followed the logarithmic relation, $u^+ = 11.7 \ln y^+ - 17$, and was independent of the chemical identity of the polymer used [16], [17]. Where $u^+ = u/u^*$,

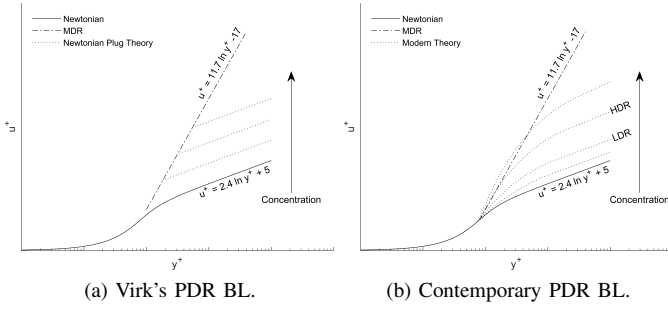


Figure 1: Demonstrating the effect of dilute polymer in the boundary layer.

$y^+ = yu^*/\nu$, and u^* is the friction velocity. Intermediate drag reduction between these two extremes is known as a Newtonian plug, also shown in Figure 1a, having the same slope, $1/\kappa$, as the Newtonian von Karman law [15]–[17]. This classically presented relative increase of mean velocity above the Newtonian law of the wall is the PDR phenomenon [17].

The velocity distributions shown in Figure 1a, thought to be well understood after 50 years of research, have been challenged in the last two decades with the advent of laser-based experiments and direct numerical simulation (DNS) [18], [19]. White et al. [18] challenged the certainty of the MDR and the validity of von Karman's constant with increased levels of drag reduction because the original empirical fits do not correlate well with the new data. This contemporary theory of PDR is demonstrated in Figure 1b, with the significant change being a blended region in place of the logarithmic elastic sublayer proposed by Virk [15], [16]. At higher levels of PDR, it was found that the profile may even exceed the MDR [18]. White et al. [18] found differences between the DNS and experimental data at the same percent drag reduction (%DR), which suggested that there may be a dependence of κ on Reynolds number or the chemical polymer [19]. Though authors such as Elbing et al. [19] suggest that further examination through a broader range of Reynolds numbers is needed before making any conclusions.

Experiments by Warholic et al. [20] suggest that there are two drag reduction regimes, low drag reduction (LDR) and high drag reduction (HDR), nominally divided at 40%DR [19], [21]. White et al. [18] suggests that the LDR/HDR separation occurs at %DR where the inertially dominated log layer is eradicated. It has been found that for LDR, the Newtonian κ remains relatively constant with the intercept constant scaling linearly with drag reduction up to %DR $\leq 30\%$ as follows, $B = 5 + (0.2)(\%DR)$ [19]. This shifts the profile vertically as classically assumed, with the drag reduction being determined by, $\%DR = \left(\frac{\tau_{w0} - \tau_w}{\tau_{w0}}\right) \times 100$, where τ_{w0} and τ_w are the Newtonian and drag reduced solution shear stresses respectively. For the HDR regime, it was found that κ did not remain constant and decreased with increasing %DR, rapidly driving the logarithmic region's intercept constant, B , towards the MDR [18], [19]. Whether the logarithmic region exists or

not in the HDR regime or at what %DR it disappears within the HDR regime has not been conclusively determined.

The bulk of PDR research focuses on internal flow in pipes and channels; fewer external flow experiments exist. Elbing et al. [19], performed boundary layer experiments where polymer injection over a flat plate is conducted in the U.S. Navy's re-circulating $5300m^3$ William B. Morgan Large Cavitation Channel (LCC) [22]. Optical particle image velocimetry (PIV) was used to produce high Reynolds number mean velocity profiles for near-zero pressure gradient [19] turbulent boundary layers. The drag force on the plate was measured using skin-friction balances. These nondimensionalized velocity profiles, quantified based on %DR by [19] will be used for comparison in the present research.

III. CFD METHODOLOGY

Simulations in the present research were conducted on a 2D flat plate domain. The incompressible, steady state, 2D x-momentum, Reynolds-averaged Navier-Stokes (RANS) equation was solved,

$$u \frac{\partial u}{\partial x} + v \frac{\partial u}{\partial y} = \nu \frac{\partial^2 u}{\partial y^2} + \nu_t \frac{\partial^2 u}{\partial y^2} \quad (1)$$

for a zero pressure gradient flat plate allowing for the pressure term to be conveniently neglected. Equation 1, was then discretized using a scheme inspired by Schetz and Bowersox [23], differing in that it is derived for use on a variable y-axis grid. The velocity convection terms were discretized with a backwards differencing scheme,

$$\frac{\partial u}{\partial x} \Big|_{x_i, y_j} \approx \left[\frac{u_{i,j} - u_{i-1,j}}{\Delta x} \right] \quad (2)$$

$$\frac{\partial u}{\partial y} \Big|_{x_i, y_j} \approx \left[\frac{u_{i,j} - u_{i,j-1}}{y_{i,j} - y_{i,j-1}} \right] \quad (3)$$

and the molecular viscous dissipation term discretized with a central differencing scheme,

$$\frac{\partial}{\partial y} \left(\nu \frac{\partial u}{\partial y} \right) \Big|_{x_i, y_j} \approx \frac{\nu}{y_{i,j+1/2} - y_{i,j-1/2}} \left(\frac{u_{i,j+1} - u_{i,j}}{y_{i,j+1} - y_{i,j}} - \frac{u_{i,j} - u_{i,j-1}}{y_{i,j} - y_{i,j-1}} \right). \quad (4)$$

The discretization scheme indexing is shown in Figure 2.

The RANS eddy viscosity term,

$$\nu_t = l_m^2 \left| \frac{\partial u}{\partial y} \right| \quad (5)$$

when discretized becomes,

$$\nu_t \Big|_{x_i, y_{j+1/2}} \approx l_{m,i,j+1/2}^2 \frac{|u_{i-1,j+1} - u_{i-1,j}|}{y_{i-1,j+1} - y_{i-1,j}} \quad (6)$$

$$\nu_t \Big|_{x_i, y_{j-1/2}} \approx l_{m,i,j-1/2}^2 \frac{|u_{i-1,j} - u_{i-1,j-1}|}{y_{i-1,j} - y_{i-1,j-1}} \quad (7)$$

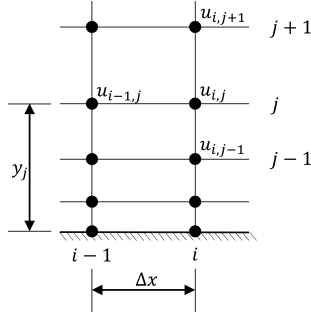


Figure 2: Grid diagram of the discretization scheme indexing.

and is modeled with a mixing length turbulence model found in Versteeg and Malalasekera [24] for a flat plate boundary layer,

$$l_m = \begin{cases} \kappa y (1 - \exp(-y^+/A)), & \text{for } y/\delta_{BL} < 0.09 \\ 0.09 \delta_{BL}, & \text{for } 0.09 \leq y/\delta_{BL} \end{cases} \quad (8)$$

with a switching point, selected at 9% of y/δ_{BL} [25], for the uniform distribution. For a Newtonian fluid, the empirical fit parameters are $\kappa = 0.41$ and $A = 26$. The RANS turbulent contribution is discretized as,

$$\frac{\partial}{\partial y} \left(\nu_t \frac{\partial u}{\partial y} \right) \Big|_{x_i, y_j} \approx \frac{1}{(y_{i,j+1/2} - y_{i,j-1/2})} \left(\nu_{t,i,j+1/2} \left(\frac{u_{i,j+1} - u_{i,j}}{y_{i,j+1} - y_{i,j}} \right) - \nu_{t,i,j-1/2} \left(\frac{u_{i,j} - u_{i,j-1}}{y_{i,j} - y_{i,j-1}} \right) \right) \quad (9)$$

with ν_t as defined in Equation 5 to 8.

After a non-trivial amount of algebra Equation 1, discretized with equations 2 to 9, can be simplified to the following equation,

$$-C_1(u_{i,j-1}) + C_2(u_{i,j}) - C_3(u_{i,j+1}) = (u_{i-1,j}). \quad (10)$$

The Thomas TDMA algorithm [26], as presented in Versteeg and Malalasekera [24], is used to solve Equation 10.

The 2D continuity equation,

$$\frac{\partial u}{\partial x} + \frac{\partial v}{\partial y} = 0 \quad (11)$$

is discretized using Equation 2 and,

$$\frac{\partial v}{\partial y} \Big|_{x_i, y_j} \approx \left[\frac{v_{i,j} - v_{i,j-1}}{y_{i,j} - y_{i,j-1}} \right],$$

resulting in,

$$(v_{i,j}) = (v_{i,j-1}) + (y_{i,j} - y_{i,j-1}) \left(\frac{u_{i-1,j}}{\Delta x} - \frac{u_{i,j}}{\Delta x} \right).$$

This first-order marching scheme has been found to provide excellent performance for a flat plate zero pressure gradient boundary layer, which has been verified in Figure 3. The

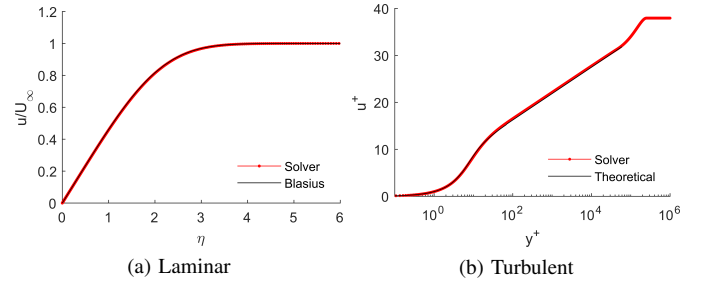


Figure 3: Verification results for the 2D momentum solver, with a laminar comparison against the Blasius curve [27] and turbulent comparison against the standard layer laws [28]. [color]

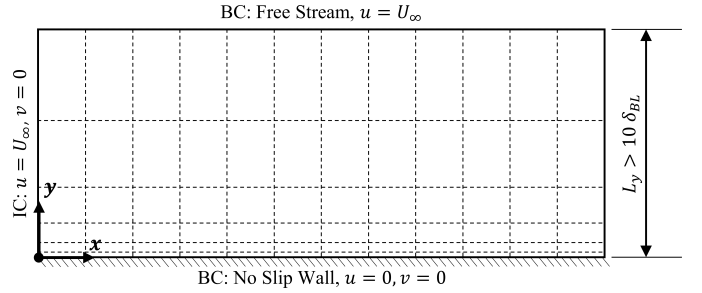


Figure 4: Flat plate grid topology shown with initial and boundary conditions. The grid used for simulation in the following section is more refined than shown here.

laminar performance of the scheme is verified against the flat-plate Blasius relation [27] (with $\nu_t = 0$) and in turbulent flow the universal law of the wall [28], [29],

$$u^+ = \frac{1}{\Lambda} \left[\frac{1}{3} \ln \frac{\Lambda y^+ + 1}{\sqrt{(\Lambda y^+)^2 - \Lambda y^+ + 1}} + \frac{1}{\sqrt{3}} \left(\arctan \frac{2\Lambda y^+ - 1}{\sqrt{3}} + \frac{\pi}{6} \right) \right] + \frac{1}{4\kappa} \ln(1 + \kappa C y^{+4}) \quad (12)$$

where $\Lambda = 0.127$, $\kappa = 0.41$, and $C = 1.43 \times 10^{-3}$. The solver performs excellently against these benchmarks with a sufficiently fine grid. The higher-order implicit schemes developed by Parr [30], as shown in Schetz and Bowersox [23], was also tested for this case but were not found to provide additional accuracy while also being more computationally demanding.

Simulations were conducted for a rectangular grid topology, as shown in Figure 4. The boundary conditions (BC) used are a no-slip wall and free stream velocity at the top of the domain. The initial condition (IC) was set to the free stream velocity.

Simulating drag reduction is accomplished through the modification of the constants κ and A of the mixing length turbulence model in Equation 8. Lowering κ increases the slope for the logarithmic region, and increasing A raises

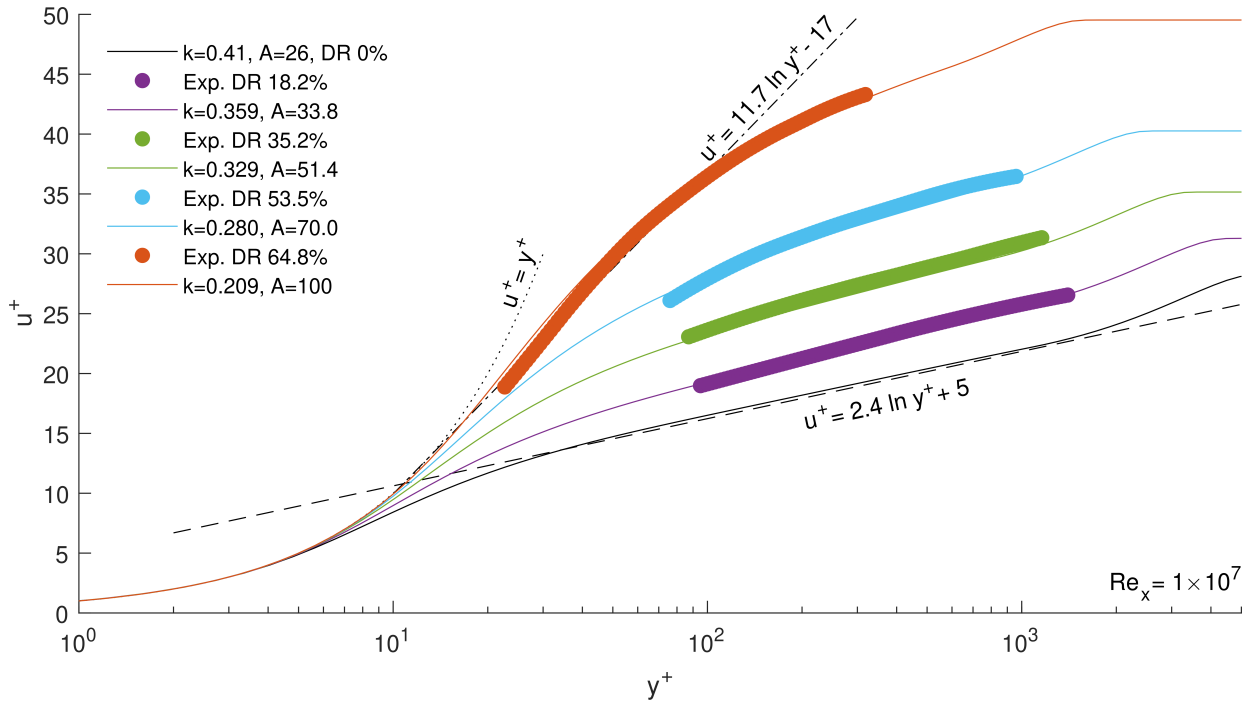


Figure 5: Simulated PDR with experimental boundary layer data for DR 18.2%, 35.2%, 53.5%, and 64.8% digitized from Elbing et al. [19]. Values of κ and A were fit to the data. [color]

the y-axis intercept. The values of κ and A , as shown in Figure 5, have been fit to experimental data from Elbing et al. [19]. Similar mixing length approaches have previously been employed by Vasetskaya and Ioselevich [31], Spalding [32], and Hecht [33] for pipe flows; and Dimant and Poreh [34] for heat transfer in drag-reducing fluids. These authors created functions by incorporating various flow properties such as friction velocity, u^* , elongational viscosity, μ_e , and those of non-Newtonian power-law fluids such as the power-law index, n , and flow consistency constant, K , into the mixing length formula. The present simulations are compared against current data collected with PIV and skin-friction balances by [19], data unavailable in the time period of the aforementioned author's publications.

IV. RESULTS & DISCUSSION

The boundary layer experimental results of Elbing et al. [19] have been reproduced in simulation through the adjustment of empirical constants in the turbulence model, shown in Figure 5. Accurate reproduction is achieved for 18.2%DR and 35.2%DR, with the 53.5%DR and 64.8%DR profiles less accurate.

With the non-dimensional profiles adequately matched and corresponding constants determined, this allows the boundary layer and wall velocity to be plotted for an external flow, as shown in Figure 6. The boundary layer velocity follows the trend of increased drag reduction, moving the profile towards that of a laminar profile. This is the result of an overall decrease in the magnitude of the turbulent eddy viscosity

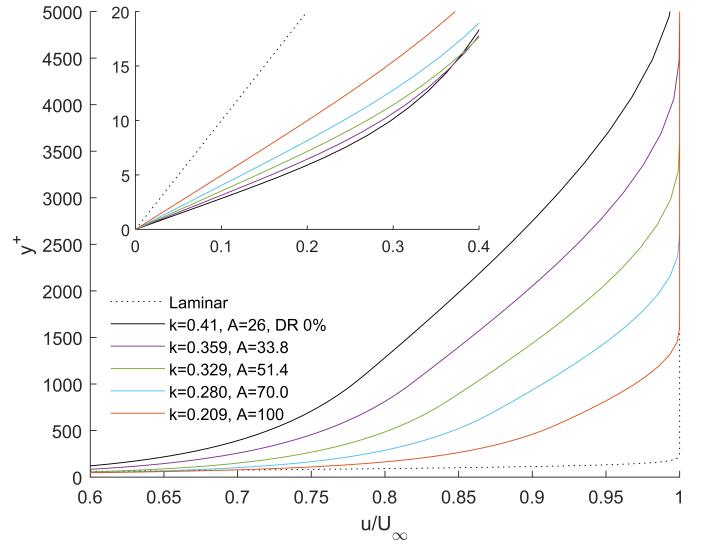


Figure 6: Velocity profiles in a boundary layer for simulated PDR at various drag reduction levels. Plot colors are congruent with Figure 5. [color]

throughout the boundary layer, as shown in Figure 7. The Reynolds stresses are represented in the RANS equations as turbulent eddy viscosity, which drive the additional viscous x-momentum dissipation sustained by turbulent flows; this is converted to y-momentum through the continuity equation. Through the general decrease in the magnitude of the eddy

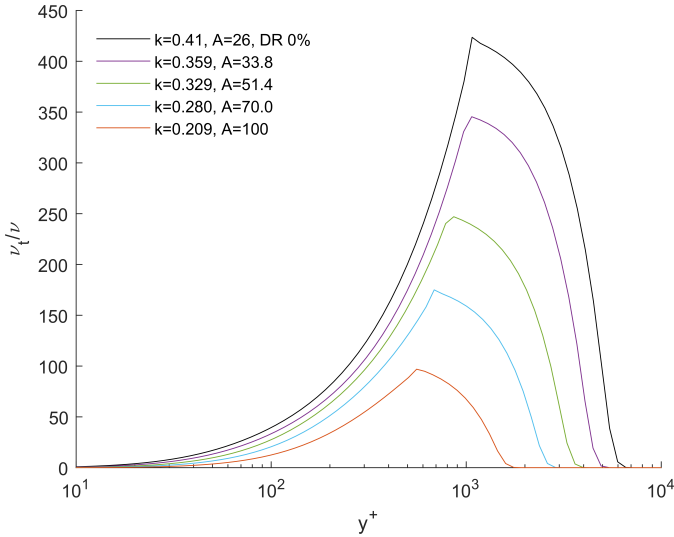


Figure 7: Eddy viscosity for simulated PDR at various drag reduction levels in a boundary layer. Plot colors are congruent with Figure 5. [color]

Table I: Comparison of boundary layer experimental and simulated drag reduction for the correlated constants κ and A .

Exp. DR	Sim. DR	Error	κ	A
-	0%	-	0.41	26
18.2%	18.2%	0%	0.359	33.8
35.2%	35.2%	0%	0.329	51.4
53.5%	50.6%	5.42%	0.280	70.0
64.8%	67.4%	4.01%	0.209	100

viscosity, the turbulent profile is driven closer to that of a laminar profile.

The velocity at the wall, plotted in Figure 6, clearly shows that for an external flow with constant free stream velocity, the velocity gradient at the wall must decrease to accommodate the drag reduction, as U_∞ is fixed, unlike in pipe flow where the centerline velocity may increase. The wall shear stress decrease is quantified in table I, where the simulated results are accurate for LDR, nominally divided at $\%DR \leq 40$, but deteriorate for the cases of HDR.

The impact of modifying the empirical constants (κ and A) on the velocity profile and eddy viscosity has been demonstrated in Figure 6 and 7 respectively. First, the individual contribution of von Karman's constant, κ , through a decrease, results in an increase in the slope of the log layer, $1/\kappa$, and a reduction in the rate of growth of eddy viscosity, ν_t , throughout the log layer. This shifts the maximum point of ν_t to larger y^+ values, slightly elongating the log layer. Secondly, increasing the value of A decreases the overall magnitude of ν_t . Both reduce the overall magnitude of ν_t , essentially allowing the profile to become more similar to a laminar profile. In the RANS equations, the Reynolds stresses represented as ν_t , drive the vertical momentum in the boundary layer. Thus, the suppression of the Reynolds

stresses, through polymer stretching, is believed to increase the momentum in the log layer relative to the sublayer [17]. Drag reduction is often discussed in the literature as an effective viscosity, which for the present work, must manifest as a reduction of ν_t , as shown in Figure 7. Thus, within the context of the RANS equations the total viscosity is of the form $\nu_{total} = \nu + (\nu_t - \nu_{eff})$. Therefore, a methodology to reduce ν_t as a function of polymer concentration will be vital in simulating an ablative polymer.

One possible approach, in turbulent flow, for available CFD solvers is the wall function. In CFD simulation, coarser grids that have the first node within the log layer require a wall function for accurate solutions as the linear differencing available to fine grids, with the first nodes within the sublayer, is not available. This function replaces the linear differencing found in an integrated wall approach with a known solution derived from the empirical profile of a flat plate boundary layer. In equation form u^* is modelled as [25], [35], [36],

$$u^* = \left[(u_{vis}^*)^4 + (u_{log}^*)^4 \right]^{1/4} \quad (13)$$

$$u_{vis}^* = \sqrt{\frac{\tau_w}{\rho}} \quad (14)$$

$$u_{log}^* = \frac{u}{\frac{1}{\kappa} \ln(y^+) + B} \quad (15)$$

where the linear u_{vis}^* and non-linear u_{log}^* components are blended by a 4th power, which is dominated by one subcomponent dependant on the y^+ of the first node.

Another possible approach is that of wall roughness. Rough walls in CFD are modeled through a downward shift in the y -axis intercept of the log layer [23], [35],

$$u^+ = \frac{1}{\kappa} \ln(y^+) + B - \Delta B \quad (16)$$

where ΔB is a function of wall roughness. PDR has the opposite effect, analogous to the "smoothing" of an already effectively smooth wall. In this analogy, PDR is effectively a negative ΔB .

Using either the wall function or wall roughness method will give access to the log law constant B , which the present author has shown to allow for the reproduction of PDR experiments closely within the LDR regime, which is the regime of interest for simulations of PDR for AUVs. This provides a potential avenue for implementation into existing CFD solver frameworks.

V. CONCLUSION

In the present work, simulations have been performed to reproduce the experimental PDR results of Elbing et al. [19] for boundary layers. This was performed by modifying empirical constants in the simple mixing length turbulence model. Accurate reproduction at LDR against experimental results supports that the simulated wall velocity profiles are adequately accurate to represent polymer drag reduction for external flows. The present work has confirmed that the expected decrease in wall shear stress will be reflected in

simulation using this approach. The wall function and wall roughness models are two potential avenues for implementing PDR into existing CFD frameworks. The empirical constants of the log law can be made into functions of local concentration, $\kappa(C)$ and/or $B(C)$.

REFERENCES

- [1] B. N. Semenov, "The of combination polymer, compliant wall and microbubble drag reduction schemes," in *International Symposium on Seawater Drag Reduction (ISSDR)*, vol. 1, 1998, pp. 269–275, Newport, RI, USA.
- [2] J. L. Zakin, J. Myska, and Z. Lin, "Similarities and differences in drag reduction behavior of high polymer and surfactant solutions," in *International Symposium on Seawater Drag Reduction (ISSDR)*, vol. 1, 1998, pp. 277–280, Newport, RI, USA.
- [3] B. R. Elbing, E. S. Winkel, M. J. Solomon, and S. L. Ceccio, "Degradation of homogeneous polymer solutions in high shear turbulent pipe flow," *Exp. Fluids*, vol. 47, pp. 1033–1044, 2009.
- [4] I. Lee and H. Park, "Prediction and verification of full-scale ship performance of frictional drag reduction coating," in *10th International Symposium on Turbulence and Shear Flow Phenomena (TSFP10)*, 2017, Chicago, IL, USA.
- [5] P. R. Resende, K. Kim, B. A. Younis, R. Sureshkumar, and F. T. Pinho, "A FENE-P $k - \epsilon$ turbulence model for low and intermediate regimes of polymer-induced drag reduction," *J. Non-Newtonian Fluid Mech.*, vol. 166, pp. 639–660, 2011.
- [6] P. R. Resende, F. T. Pinho, B. A. Younis, K. Kim, and R. Sureshkumar, "Development of a low-Reynolds-number $k - \omega$ model for FENE-P fluids," *Flow, Turbul. Combust.*, vol. 90, pp. 69–94, 2013.
- [7] M. Masoudian, K. Kim, F. T. Pinho, and R. Sureshkumar, "A Reynolds stress model for turbulent flow of homogeneous polymer solutions," *Int. J. Heat Fluid Flow*, vol. 54, pp. 220–235, 2015.
- [8] P. R. Resende, A. M. Afonso, and D. O. Cruz, "An improved $k - \epsilon$ turbulence model for FENE-P fluids capable to reach high drag reduction regime," *Int. J. Heat Fluid Flow*, vol. 73, pp. 30–41, 2018.
- [9] R. Y. Hou, S. Peng, Y. Xiong, and D. Yang, "Influence of polymer additive on flow past an underwater slender body," in *IEEE 8th International Conference on Underwater System Technology: Theory and Application (USYS)*, 2018, Wuhan, HB, China.
- [10] J. J. White, A. G. L. Holloway, and T. L. Jeans, "Methodology for simulating ablative polymer mass transport at very large Schmidt numbers for polymer drag reduction," in *29th Annual Conference of the Computational Fluid Dynamics Society of Canada (CFDSC)*, 2021, St. John's, NL, Canada [Online].
- [11] B. A. Toms, "Some observations on the flow of linear polymer solutions through straight tubes at large Reynolds numbers," in *International Congress on Rheology*, 1948, pp. 135–141, Scheveningen, SH, Holland.
- [12] W. A. Meyer, "A correlation of the frictional characteristics for turbulent flow of dilute viscoelastic non-Newtonian fluids in pipes," *A.I.Ch.E. Journal*, vol. 12, no. 3, pp. 522–525, 1966.
- [13] C. Elata, I. Lehrer, and A. Kahanovitz, "Turbulent shear flow of polymer solutions," *Isr. J. Technol.*, vol. 4, 1966.
- [14] S. Hassid and M. Poreh, "A turbulent energy model for flows with drag reduction," *J. Fluids Eng.*, vol. 97, no. 2, pp. 234–241, 1975.
- [15] P. S. Virk, H. S. Mickley, and K. A. Smith, "The ultimate asymptote and mean flow structures in Toms' phenomenon," *J. Appl. Mech.*, vol. 37, no. 2, pp. 488–493, 1970.
- [16] P. S. Virk, "Drag reduction fundamentals," *AICHE J.*, vol. 21, no. 4, pp. 625–656, 1975.
- [17] V. S. L'vov, A. Pomyalov, I. Procaccia, and V. Tiberkevich, "Drag reduction by polymers in wall bounded turbulence," *Phys. Rev. Lett.*, vol. 92, no. 24, p. 244503, 2004.
- [18] C. M. White, Y. Dubief, and J. Klewicki, "Re-examining the logarithmic dependence of the mean velocity distribution in polymer drag reduced wall-bounded flow," *Phys. Fluids*, vol. 24, no. 2, p. 021701, 2012.
- [19] B. R. Elbing, M. Perlin, D. R. Dowling, and S. L. Ceccio, "Modification of the mean near-wall velocity profile of a high-Reynolds number turbulent boundary layer with the injection of drag-reducing polymer solutions," *Phys. Fluids*, vol. 25, no. 8, p. 085103, 2013.
- [20] M. D. Warholic, H. Massah, and T. J. Hanratty, "Influence of drag-reducing polymers on turbulence: effects of Reynolds number, concentration and mixing," *Exp. Fluids*, vol. 27, pp. 461–472, 1999.
- [21] Y. Dubief, "Numerical simulation of high drag reduction in a turbulent channel flow with polymer additives," Center for Turbulence Research, Stanford University, CA, USA, Tech. Rep., 2003.
- [22] R. J. Etter, J. M. Cutbirth, S. L. Ceccio, D. R. Dowling, and M. Perlin, "High Reynolds number experimentation in the US Navy's William B Morgan large cavitation channel," *Meas. Sci. Technol.*, vol. 16, pp. 1701–1709, 2005.
- [23] J. A. Schetz and R. D. W. Bowersox, *Boundary Layer Analysis*, 2nd ed. American Institute of Aeronautics and Astronautics (AIAA) Inc., 2011.
- [24] H. K. Versteeg and W. Malalasekera, *An Introduction to Computational Fluid Dynamics The Finite Volume Method*, 2nd ed. Pearson, 2007.
- [25] D. C. Wilcox, *Turbulence Modeling for CFD*, 3rd ed. DCW Industries, 2006.
- [26] L. H. Thomas, "Elliptic problems in linear differential equations over a network," Watson Scientific Computing Laboratory, Columbia University, New York, NY, USA, Tech. Rep., 1949.
- [27] F. M. White, *Viscous Fluid Flow*, 3rd ed. McGraw-Hill, 2006.
- [28] H. Schlichting and K. Gersten, *Boundary-Layer Theory*, 9th ed. Springer-Verlag, 2017.
- [29] K. Gersten and H. Herwig, *Strömungsmechanik: Grundlagen der Impuls-, Wärme- und Stoffübertragung aus asymptotischer Sicht*. Vieweg-Verlag, 1992.
- [30] W. Parr, "Laminar boundary layer calculations by finite differences," Naval Ordnance Lab., White Oak, MD, USA, Tech. Rep., 1963.
- [31] N. G. Vasetskaya and V. A. Ioselevich, "Semiempirical turbulence theory for dilute polymer solutions," *Fluid Dyn.*, vol. 5, pp. 289–296, 1970.
- [32] D. B. Spalding, "A model and calculation procedure for the friction and heat transfer behaviour of dilute polymer solutions in turbulent pipe flow," in *Progress in Heat and Mass Transfer*. Pergamon, 1972, pp. 275–284.
- [33] A. M. Hecht, "A turbulent mixing length formulation for non-Newtonian power law fluids," *J. Hydronautics*, vol. 6, no. 1, pp. 21–26, 1972.
- [34] Y. Dimant and M. Poreh, "Heat transfer in flows with drag reduction," in *Advances in Heat Transfer*. Elsevier, 1976, pp. 77–113.
- [35] Ansys Inc., *ANSYS CFX Solver Theory Guide*, 2016.
- [36] S. B. Pope, *Turbulent Flows*. Cambridge University Press, 2000.